Magnetocaloric properties of TbCrO₃ and TmCrO₃ and their comparison with those of the other $RCrO_3$ systems (R = Gd, Dy, Ho, and Er)

Cite as: J. Appl. Phys. 134, 103903 (2023); doi: 10.1063/5.0153110 Submitted: 4 April 2023 · Accepted: 27 August 2023 · Published Online: 13 September 2023







Jianhang Shi, ^{1,2} 🔟 Mohindar S. Seehra, ³ 🕩 Jacob Pfund, ⁴ 🕩 Shiqi Yin, ⁴ 🕩 and Menka Jain^{2,4,a)} 🕩



AFFILIATIONS

- Department of Materials Science and Engineering, University of Connecticut, Storrs, Connecticut 06269, USA
- ²Institute of Materials Science, University of Connecticut, Storrs, Connecticut 06269, USA
- 3 Department of Physics and Astronomy, West Virginia University, Morgantown, West Virginia 26506, USA
- ⁴Department of Physics, University of Connecticut, Storrs, Connecticut 06269, USA

ABSTRACT

Magnetocaloric properties of TbCrO₃ and TmCrO₃ are reported and compared with those of the previously reported rare-earth chromites $\overset{\pm}{0}$ RCrO₃ (R = Gd, Dy, Ho, and Er) and other perovskite-type oxides. The samples of TbCrO₃ and TmCrO₃ in this work were synthesized using a citrate gel combustion technique, and their magnetic properties were investigated and compared with those reported previously on $RCrO_3$ (R = Gd, Dy, Ho, and Er). The Cr^{3+} - Cr^{3+} ordering temperatures were found to strongly depend on the ionic radii of the rare-earth. By fitting the dc magnetization data with modified Curie–Weiss law including the Dzyaloshinsky–Moriya antisymmetric exchange interaction (D) and the symmetric exchange constant I_e , spin canting angles (α) were obtained. In general, α was found to increase with the decreasing ionic radii of R^{3+} in RCrO₃. The magnetocaloric properties investigated included the magnetic entropy change $(-\Delta S)$ for a $\frac{\omega}{6}$ given change in magnetic field (ΔH), the corresponding adiabatic temperature change (ΔT_{ad}), and their relative variations ($\Delta T_{ad}/\Delta H$) and $(-\Delta S/\Delta H)$. It is observed that for RCrO₃, $(-\Delta S)$ measured in the vicinity of the ordering temperature of $R^{3+}-R^{3+}$, varies almost as $G^{2/3}$ where G is the de Gennes factor. Among RCrO₃, GdCrO₃ shows the largest value of (-ΔS/ΔH), because of its largest G factor and its magnitudes of $(\Delta T_{ad}/\Delta H)$ and $(-\Delta S/\Delta H)$ compare well with the reported values for the perovskites GdFeO₃ and EuTiO₃. These comparisons presented here provide useful information on the potential use of these materials in magneto-refrigeration technology.

Published under an exclusive license by AIP Publishing. https://doi.org/10.1063/5.0153110

I. INTRODUCTION

Rare-earth chromites with the general formula of RCrO₃ (R = Gd, Tb, Dy, Ho, Er, and Tm) have recently received considerable attention due to their noteworthy properties for potential applications as oxygen ion conductors, interconnect materials for solid oxide cells, UV photonic devices, magnetic refrigerant, gas sensors, and multiferroics. 1-3 The chromites are isostructural and adopt a centrosymmetric orthorhombic structure with space group Pbnm (No. 62). They are p-type semiconductors at room temperature and exhibit a high conductivity at high temperatures.^{2,3,5} Recent studies have also indicated that certain rare-earth chromites belong to a new family of ferroelectric and antiferromagnetic multiferroics^{2,6} although the origin and ferroelectric transition

temperature are still under debate. The initially claimed ferroelectric transition temperature (472-516 K) has nowadays been observed just above T_N^{Cr} . 7-9 For example, the onset of polar order of HoCrO₃ was recently observed to be 240 K instead of the previously claimed 472 K.⁹ It was proposed that the multiferroicity arises from exchange interactions between R³⁺ ions and the Cr³⁺ sublattice or special spin configuration. 6,10,11

The novel magnetic properties of RCrO₃, such as magnetization reversal and magnetization jump, arise from magnetic spin interactions between magnetic ions, namely, the Cr³⁺-Cr³⁺, R³⁺-R³⁺, and Cr3+-R3+ interactions, which are isotropic, symmetric, and antisymmetric anisotropic, respectively. 7,12 Consequently, RCrO₃ exhibits three magnetic transitions: the antiferromagnetic (AFM) Cr³⁺ sublattice ordering, spin reorientation, and R³⁺ sublattice

a)Author to whom correspondence should be addressed: menka.jain@uconn.edu

ordering. The Cr³⁺-ordering temperature of RCrO₃ is observed to shift to higher values with the increasing ionic radii of the R-ion. This evolution of magnetic or transport properties is also observed in other rare-earth oxides, which could be correlated to the steric effects due to the lanthanide contraction. 13 For example, the Mn ordering temperature of RMnO₃ was observed to decrease with the reduction of the ionic radii of R-ion as it influences the Mn-O-Mn bond angle and hence the Mn-Mn exchange modifies. 14 A sharp metal-to-insulator transition in RNiO₃ is also found to be dependent on the Ni-O-Ni bond angle. ¹⁵ Moreover, in such oxides, it has been observed that the multifunctional properties, such as magnetocaloric effect (MCE), magnetoelectric effect, and multiferroic properties, strongly depend on the magnetic interaction between the 4f rare-earth ions and 3d transition metal ions. 16 Thus, it can be inferred that the physical properties of the rare-earth oxides could be modulated by a number of parameters including, but not limited to, ionic radii of the R-ion, chemical (substitution) or external pressure, and epitaxial strain engineering.

The magnetocaloric effect, which is a change in the temperature of a material by the application of magnetic field, can be evaluated as an adiabatic temperature change (ΔT_{ad}) of a material in the adiabatic limit or magnetic entropy change (ΔS) in the isothermal limit. The isothermal heat $Q = T\Delta S$ represents the heat pumped in cooling and heating cycles in magnetic refrigeration, where T is the temperature. The giant MCE was first discovered in Gd₅(Si₂Ge₂) in the late 1990s by Pecharksy and Gschneidner. 18 The magnetic entropy change was 13 J/kg K under a magnetic field change of 2 T (20 k Oe), which was about 50% larger than the previously known largest magnetic entropy change in Gd metal. A large ΔS can be extracted from a magnetic material by sweeping an external magnetic field and using a temperature near magnetic transition. A few recent studies dedicated to the MCE properties of RCrO₃ exhibited large MCE at low temperatures. 16 For example, a giant MCE with a magnetic entropy change (-ΔS) of 31.6 J/kg K was observed in the GdCrO₃ single crystal with a field change (ΔH) of 4.4 T.¹² Selective rare-earth doping at the R-site of RCrO3 has been explored to optimize the MCE properties. 17,19 Our recent studies on HoCrO₃ and GdCrO₃ suggest that MCE could also be tuned by controlling the particle size. 4,20 The MCE of the thin RCrO₃ film has also been investigated and compared with its bulk sample.21,22 However, the study of evolution of MCE properties of RCrO3 across a series of rare-earth is still missing. With the variation of R ions, one can perform systematic studies of not only MCE in this family of materials but also magnetic behavior that depends on the interplay of 3d and 4f magnetism.²³ A comprehensive and comparative study throughout the R series may offer the possibility to reveal general criteria of large MCE and other physical properties in the RCrO₃ family. Therefore, in this paper, we report magnetic and magnetocaloric properties of TbCrO3 and TmCrO3 to complete our investigations of the rare-earth chromites which also enables us to present a comparative study of the magnetic and magnetocaloric properties of the RCrO₃ (R = Gd, Tb, Dy, Ho, Er, and Tm) system with a focus on the general trends and relationships between the MCE and ionic radii of the R³⁺-ions. We also provide a comparison of these properties of RCrO₃ with reported properties of other perovskite oxides such as RMnO₃ (R = Ho, Dy, Tb, and Yb), EuTiO₃,

GdFeO₃, and GdCoO₃ to determine the best materials for potential magnetocaloric applications.

II. EXPERIMENTAL

In our previous studies, we described the synthesis of polycrystalline bulk powder samples of RCrO3 using a citrate gel combustion technique. 4,17,20,24 In this method, high purity (99.999%) nitrate precursors of Gd, Tb, Dy, Ho, Er, Tm, and Cr along with citric acid were dissolved in water separately. The solutions were then mixed in a desired stoichiometric ratio and dried until combustion. The resultant powders were annealed at 900 °C in oxygen for 2h to form GdCrO₃, TbCrO₃, DyCrO₃, HoCrO₃, ErCrO₃, and TmCrO₃ bulk powders (hereafter referred as GCO, TbCO, DCO, HCO, ECO, and TmCO, respectively). In this work, the samples of TbCO and TmCO were newly synthesized, and their magnetic properties were measured using a vibrating sample magnetometer (VSM) option attached to an Evercool Physical Property Measurement System from Quantum Design. Their measured properties were then compared with those of other rare-earth chromites RCrO₃ (R = Gd, Dy, Ho, and Er) presented in our previous and results from this comparative investigation of the six chromites are reported here.

III. RESULTS AND DISCUSSIONS

A. Temperature dependence of magnetization

The temperature dependence of zero-field-cooled (ZFC) and $\frac{1}{4}$ field-cooled (FC) dc magnetization data (M-T) measured with an applied field of 50 Oe for all RCrO₃ samples studied here are illustrated in Fig. 1. $^{4.17,20,24}$ These M-T curves reveal complex magnetic properties in RCrO₃. Magnetization evolution for the six samples exhibits one transition point around 150 K, either in ZFC or FC modes, which is attributed to a transition from the high-

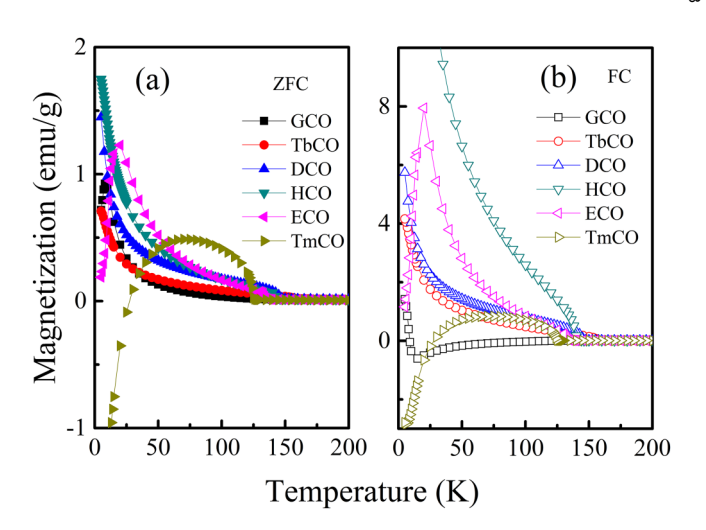


FIG. 1. Temperature dependence of the (a) zero-field-cooled (ZFC) and (b) field-cooled (FC) dc magnetization for $RCrO_3$ at an applied dc magnetic field of H=50 Oe.

temperature paramagnetism to the lower temperature antiferromagnetism of Cr^{3+} sublattice below T_N^{Cr} . Other transitions observed for some RCrO₃ at around 20 K could be attributed to spin reorientation. In all RCrO₃ samples, the magnetic moments of Cr³⁺ ions order antiferromagnetically with a typical G-type magnetic structure below T_N^{Cr} . Temperature dependent FC data of GCO and TmCO reveal temperature-induced magnetization reversal at the compensation temperature of T_{com} ~130 and ~30 K, respectively. The existence of T_{com} for TmCO could be attributed to the negative internal magnetic field (\sim -1500 Oe) antiparallel to the applied field, which is induced by coupling between Tm³⁺ and Cr³⁺ moments and the three singlet states of Tm3+ created by the crystalline field.²⁵ The negative magnetization for TmCO disappears when the applied magnetic field is larger than internal field. 25,26 The magnetization shows a maximum at 20 and 8 K for ECO and GCO, respectively, and, it becomes minimum at 6 K for TmCO. This phenomenon is ascribed to the spin reorientation of rare-earth ion at A-site which is induced by a balance of Zeeman energy of the applied magnetic field and anisotropy energies.²⁷ At spin reorientation temperature, the effective magnetic field on the R³⁺ ions reverses sign.²⁷ Spins overcome the anisotropic energy of the canted Cr3+ and rotated by Zeeman energy between the R5+ moments and the applied field.²⁵ For example, the ECO undergoes a magnetic transition at ~22 K from $\Gamma_4(G_xA_vF_z)$ to $\Gamma_1(A_xG_vC_z)^{\perp}$ by an effective internal field of \sim -10 kOe along the c-axis.²⁷ For GCO and TmCO, the spin reorientation results in a parallel direction of R³⁺ moments to the applied filed.²⁶ As for TbCO, DCO and HCO, in both ZFC and FC modes, the M-T curves show that the magnetization increase monotonously with deceasing temperature below the Néel temperature T_N^{Cr} .

To clearly locate the transition temperature of T_N^{Cr} , the temperature derivative of the product of temperature and magnetic susceptibility ($\chi = M/H$) is plotted and presented in Fig. 2(a).^{4,17,2}

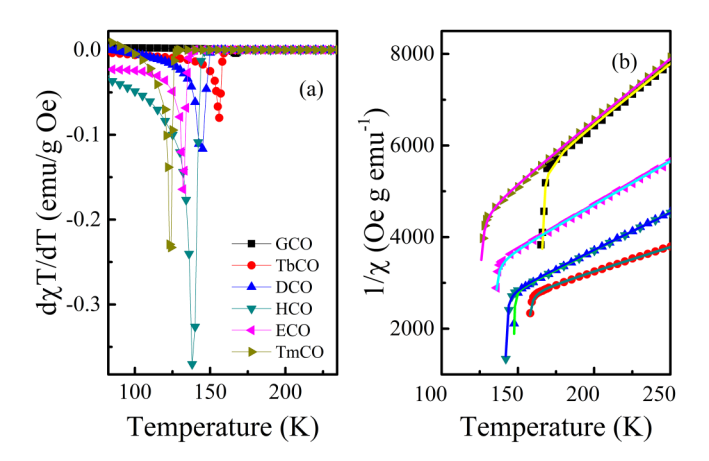


FIG. 2. (a) Temperature dependence of the derivative of the product of temperature (T) and magnetic susceptibility (χ) with respect to the temperature for RCrO₃. (b) The plots of field-cooled $1/\chi$ vs T for the RCrO₃ samples with the solid lines as fitting of the data to the modified Curie-Weiss equation [Eq. (1)]. The parameters obtained from these fits are listed in Table I.

From the position of the peaks, $T_N^{cr} = 167$, 156, 145, 138, 132, and 124 K are determined for GCO, TbCO, DCO, HCO, ECO, and TmCO, respectively. These values are also listed in Table I. For temperatures well above T_N^{Cr} , all samples of RCrO₃ show clear Curie-Weiss behavior since plots of $1/\chi$ vs T are linear as evident in Fig. 2(b). However, on approach to T_N^{Cr} , there are strong departures from this linear behavior, which has been explained to be due to the presence of the antisymmetric Dzyaloshinsky-Moriya (DM) interaction between the Cr3+ ions. In this case, the modified Curie-Weiss law modeled by Moriya leads to the following equations:²

$$\chi = \frac{C}{(T-\theta)} \frac{T - T_0}{(T - T_N^{C_r})},\tag{1}$$

$$T_0 = \frac{2J_e ZS(S+1)}{3k_B},$$
 (2)

$$T_N^{Cr} = \frac{2J_e ZS(S+1)}{3k_B} \left[1 + \left(\frac{D}{2J_e}\right)^2 \right]^{1/2},$$
 (3)

where T_N^{Cr} is the ordering temperature of Cr^{3+} , C is the Curie constant, T_0 is a fitted parameter, θ is the Weiss temperature, k_B is the Boltzmann constant, and J_e and D are the strength of symmetric and antisymmetric exchange interactions between nearest Cr³⁺ ions, respectively. In addition, Z(Z=6) and S(S=3/2) are the coordination number and spin quantum number of Cr^{3+} , respectively. The excellent fits to Eq. (1) near T_N^{Cr} as depicted in Eq. (2(b) indicate the dominant contribution of D to the temperature variation of the magnetic susceptibility on approach to T_N^{Cr} . ture variation of the magnetic susceptibility on approach to T_N^{Cr} . The parameters obtained from these fits are listed in Table I. It has been observed that the strength of symmetric exchange interaction J_e is found to decrease systematically with the decreasing of ionic radii of rare-earth ions. More importantly, θ is negative for all samples indicating antiferromagnetic (AFM) alignment of Cr³⁺ for all RCrO₃. The magnitude of θ in ECO is significantly greater than that found in other rare-earth chromites. The sensitivity of the modified Curie-Weiss law near T_N^{Cr} may be the reason for this observation regarding the choice of data to fit. The strength of interactions θ in rare-earth magnets is typically overestimated as a result of contributions from crystal field levels that are thermally populated when fitting high-temperature paramagnetic data.² However, overestimation of θ would not necessarily impact the precision of other obtained fitting parameters, such as the effective magnetic moment.2

The effective magnetic moment $\mu_{\it eff}$ was also evaluated based on the C from the modified Curie–Weiss law according to $\mu_{eff} = \sqrt{3Ck_B/N}$, where N and the Avogadro's constant N_A are related by the equation: $N/(\text{molecular weight}) = N_A$. As listed in Table I, these calculations based on the C values obtained from the plots yield $\mu_{eff}=8.74~\mu_{B},\,11.10~\mu_{B},\,11.21~\mu_{B},\,11.46~\mu_{B},\,10.81~\mu_{B},\,$ and $8.93\,\mu_{\rm B}$ for GCO, TbCO, DCO, HCO, ECO, and TmCO, respectively. The theoretical effective moment values were also estimated based on the spin-only moment of free-ions according to $\mu_{theo} = \sqrt{\mu_{Cr}^2 + \mu_R^2}$, which are also listed in Table I. The μ_{eff} values are in close agreement with the theoretical values μ_{theo} . It should be

TABLE I. For RCrO₃, the values for the following magnetic parameters are listed: $T_{N}^{Cr'}$: Née/ temperature measured by the $d(\chi T)/dT$ method along with the Weiss temperature θ , the Néel temperature T_N^{Cr} where Cr-ions order, Curie constant C, fitting parameter T_0 , symmetric exchange constant J_e , antisymmetric exchange constant D, canting angle (α) , and the effective magnetic moment μ_{eff} , obtained from fitting the field-cooled magnetic data to the modified Curie–Weiss equation (1). Also listed is the the theoretical magnetic moment μ_{theo} .

	GCO	ТЬСО	DCO	HCO	ECO	TmCO
$T_N^{Cr'}$	167	156	145	138	132	124
$\theta(K)$	-38.95(3.31)	-38.58(6.34)	-22.0(1.24)	-31.84(5.68)	-60.99 (11.48)	-43.8(4.17)
$T_N^{Cr}(K)$	166.8 (1)	156.7 (1)	147.3 (1)	141.7 (1)	133.7 (1)	124.7 (1)
C (emu K/Oe g)	0.03710 (44)	0.05954 (133)	0.05981 (28)	0.06202 (128)	0.05469 (213)	0.03709 (56)
$T_0(K)$	166.7 (1)	156.5 (2)	147.2 (1)	141.4 (2)	133.2 (2)	124.3 (1)
J_e/k_B	11.11 (0)	10.43 (1)	9.81 (0)	9.43 (1)	8.88 (1)	8.29 (1)
D/k_B	0.77(3)	1.06 (4)	0.72(2)	1.23 (3)	1.54(2)	1.33 (2)
D/J_e	0.0693 (23)	0.1011 (34)	0.0737 (25)	0.1304 (29)	0.1735 (24)	0.1606 (27)
α (°)	1.98 (7)	2.89 (10)	2.11 (7)	3.72 (9)	4.92 (7)	4.56 (8)
$\mu_{eff}(\mu_B)$	8.74 (5)	11.10 (12)	11.21 (3)	11.46 (12)	10.81 (21)	8.93 (26)
$\mu_{theo}(\mu_B)$	8.81	10.45	11.29	11.29	10.36	8.54

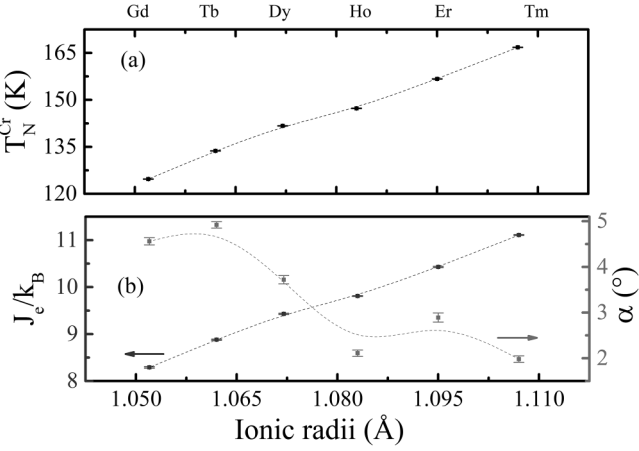
noted that this family of materials exhibit G-type AFM behavior with canted spins of Cr^{3+} . The spin canting angle (α) was estimated by the molecular filed theory based on the ratio of antisymmetric (D) to symmetric (J_e) exchange constant using the following equation: $\alpha = \frac{1}{2} \arctan(D/J_e)^{30}$ These angles, also listed in Table I, are non-zero indicate that the magnetic moments of Cr3+ are not totally antiparallel to their nearest neighbor due to the DM interaction resulting in weak ferromagnetism (WFM). Spin canting could arise due to a variety of reasons, most of which are antisymmetric DM interaction and the single-ion magnetic anisotropy.³¹ been argued that for relatively high T_N ($T_N \ge 100$ K), the canting is caused primarily for DM interactions.³¹ The magnitudes of this α varying from 1.98° for GCO to 4.92° for ECO are typical of the canting observed in other weak ferromagnets and the ones reported for some RCrO₃. ^{33,34} For example, Shamir *et al.* reported a neutron diffraction-measured spin canting angle of 3.2° in HoCrO₃³⁴ that is in agreement with our calculated $\alpha = 3.7^{\circ}$ for HoCrO₃ listed in Table I.

The evolution of several key magnetic parameters with the ionic radii of R3+, such as symmetric exchange constant, spin canting angle, and the Cr3+-Cr3+ ordering temperature obtained from modified Curie-Weiss fitting, has been plotted in Fig. 3. The value of T_N^{Cr} increases almost linearly with the increasing ionic radii of \mathbb{R}^{3+} , which is consistent with the reported variation in RCrO_3 . A similar relationship between the \mathbb{R}^{3+} ionic radii and T_N has also been reported in RMnO₃.35 Qualitatively, this phenomenon has been attributed to the dependence of the Cr-O-Cr bond angle on the size of R3+ ionic radii since the Cr-O-Cr bond angle affects the superexchange interaction of neighboring t2g electrons of Cr³⁺ ions through the DM interaction. In Fig. 3(b), the effect of ionic radii on the exchange constant and α have been revealed for the first time. The antisymmetric exchange constant does not show strong correlation with the ionic radii as listed in Table I and hence, D is not plotted in this figure. J_e/k_B increases monotonically with the ionic radii of R-ion and α decreases with ionic radii in general. This result is consistent with the observations for other Pbnm perovskites that largest canting should be present in systems

with small J_e .³⁶ An increase of the strength of symmetric $Cr^{3+}-Cr^{3+}$ interaction is reflected in the increase of T_N^{Cr} . This finding establishes direct experimental evidence of the relationship between the exchange constant and the ionic radii of rare-earth.

B. Magnetic hysteresis

Isothermal magnetization vs applied field (M−H) loops were ∓ recorded for RCrO₃ in a field sweep from -40 to $40 \text{ kOe} \stackrel{6}{\cancel{9}}$ (10 kOe = 1 T) at various temperatures. Figure 4 shows the representative isothermal M-H loops of RCrO₃ at only 5 K. Obviously, all loops depict noticeable hysteresis. The origin of the WFM component is related to the canting of Cr3+ spins due to the DM type antisymmetric exchange interaction as mentioned



ionic radii of rare-earth ions and (b) variation of the symmetric exchange constant $(J_{e}/k_{B},$ left) and spin canting angle $(\alpha,$ right) as a function of ionic radii of various R ions. The lines connecting the data points are visual guides.

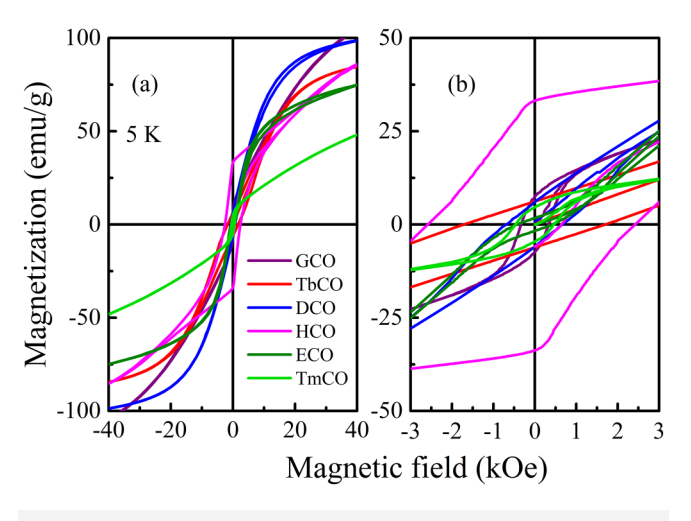


FIG. 4. (a) Magnetic field dependence of magnetization of RCrO₃ at 5 K. (b) Zoomed view of the hysteresis loops for lower fields at 5 K.

before.³⁷ For all the present samples, magnetization did not saturate up to 40 kOe but exhibited a near linear variation on approach to 40 kOe. The hysteresis loops at low fields are due to weak ferromagnetism produced by canting of the Cr3+ spins whereas the linear component has contributions from the antiferromagnetic susceptibility of the Cr3+ sublattices and the paramagnetic (antiferromagnetic) susceptibility of the R3+ ions above (below) their ordering temperatures (<10 K).^{37,38} Furthermore, as the temperature gradually increases and reaches above T_N^{Cr} , all samples show paramagnetic behavior (not shown here).

The temperature dependence of the coercive field (H_C) and remanent magnetization (M_R) extracted from the hysteresis loops is illustrated in Figs. 5(a) and 5(b), respectively. 4,17,20,24 As depicted in

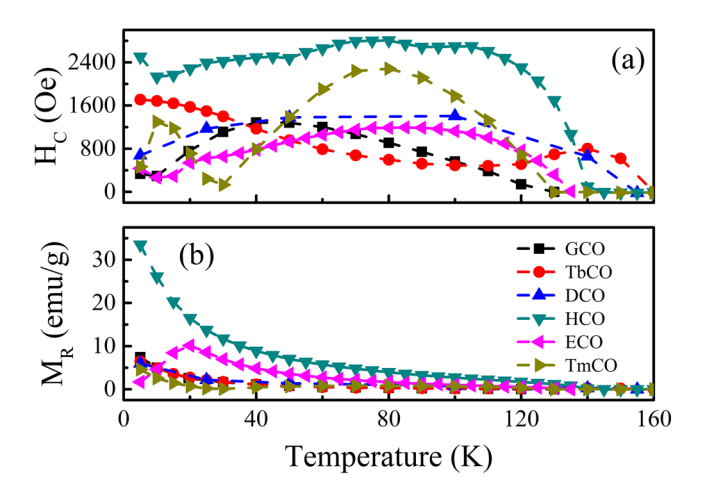


FIG. 5. The temperature dependence of (a) coercive field (H_C) and (b) remnant magnetization (M_R) of the RCrO₃ bulk samples.

Fig. 5(a), the temperature dependence of H_C shows significant difference among RCrO₃ in a temperature range of 5-160 K. In contrast, M_R was found to decrease quite rapidly with increasing temperature reaching zero at T_N^{Cr} for all the samples except that for ECO. The abnormal M_R peak of ECO at around 22 K may be attributed to the spin reorientation from Γ_4 to Γ_1 magnetic phases.³⁸ For H_C , there is a general trend in temperature dependent plot with a decreasing temperature for $T < T_N^{Cr}$: H_C first increases, then reaches a broad plateau with a further decrease in temperature, except for TmCO (before going to zero at $T \geq T_N^{Cr}$). The broad peak in the temperature dependence of H_C data has also been recently reported for some of the RCrO3, which could be qualitatively explained on the basis of superimposing Cr^{3+} and R^{3+} magnetic sublattices.³⁷ The initial increase in H_C with decreasing temperature below T_N^{Cr} is due to the contribution of Cr^{3+} sublattice. As the temperature is lowered, the weak ferromagnetic signal from the Cr³⁺ sublattice is expected to saturate and the paramagnetic contribution from the R³⁺ sublattice is expected to increase.²⁴ Therefore, the combined effect of ferromagnetic and paramagnetic contributions is expected to result in a broad plateau or decreased H_C as the temperature is further decreased.²⁴ The reason for a local minimum of TmCO in H_C at around ~28 K could be related to the reversal of the antiparallel coupling between Tm³⁺ and Cr³⁺.

Another quantity of interest in connection with magnetocaloric materials is the hysteresis loss, which is the energy dissipated in the medium and can be defined as the enclosed area inside the hysteresis loops and often simplified as the energy product $M_R \cdot H_C$.⁴ As can be seen in Fig. 4, all samples exhibit hysproduct $M_R \cdot H_C$. As can be seen in Fig. 4, all samples exhibit hysteresis loops indicating the nature of irreversible processes. The hysteresis loss calculated based on the values of H_C and M_R in Fig. 5 is plotted in Fig. 6. In general, the hysteresis loss reduces $\frac{10}{100}$

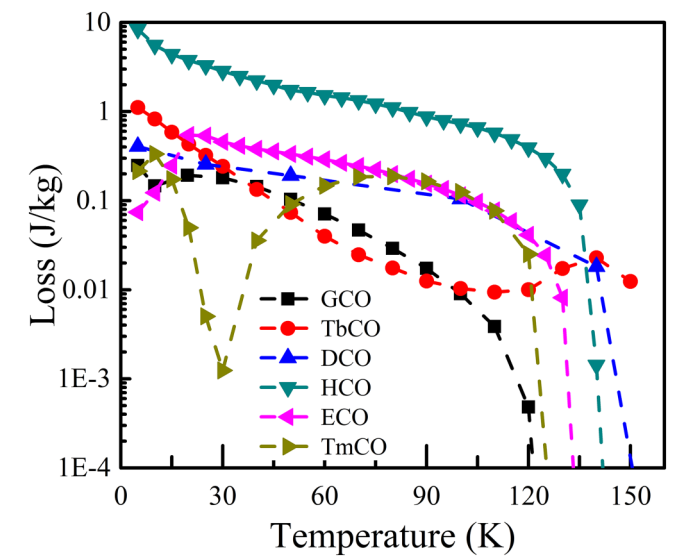


FIG. 6. Temperature dependence of hysteresis loss of the present RCrO₃ samples. The lines connecting the data points are visual guides.

quite rapidly approaching to zero at T_N^{Cr} for all the present samples. The hysteresis loss is less than 1 J/kg for all the present RCrO₃ samples except for HCO. At 5 K, the hysteresis loss values for GCO, TbCO, DCO, HCO, ECO, and TmCO are 0.25, 1.11, 0.41, 8.38, 0.07, and 0.21 J/kg, respectively. The stronger exchange interaction of $\mathrm{Ho^{3+}}$ with $\mathrm{Cr^{3+}}$ may be responsible for largest H_C , M_R , and resulting hysteresis loss in HCO.37 For the TmCO sample, the significant drop in H_C and the resulting hysteresis loss near 30 K are possibly related to the temperature-induced magnetization reversal.

C. Magnetocaloric properties

To investigate the magnetocaloric properties of the RCrO₃ samples, magnetic field dependence of the magnetization (M) in magnetic fields H from 0 to 4 T was measured for the TbCrO3 and TmCrO₃ to complement our similar measurements reported previously for the other four RCrO₃ (R = Gd, Dy, Ho, and Er).^{4,17,20,24} The magnetic entropy change $(-\Delta S)$ was then calculated based on the following equation:

$$\Delta S(T)_{\Delta H} = \int_{H_i}^{H_f} \left(\frac{\partial M(T, H)}{\partial T} \right)_H dH, \tag{4}$$

where H_i is the initial field, H_f is the final field, M(T,H) is the magnetization of sample under a magnetic field H and temperature T. Based on Eq. (4) and the plots of M vs H at different temperatures (not shown), the values of $(-\Delta S)$ of RCrO₃ were calculated for different temperatures and the results are presented in Fig. 7. These results show that maximum $(-\Delta S)$ in the plot occurs at lowest measured temperature (5 K) for GCO. For the other RCrO₃, the $(-\Delta S)$ value peaks at temperatures above 5 K. It is clearly seen in Fig. 7

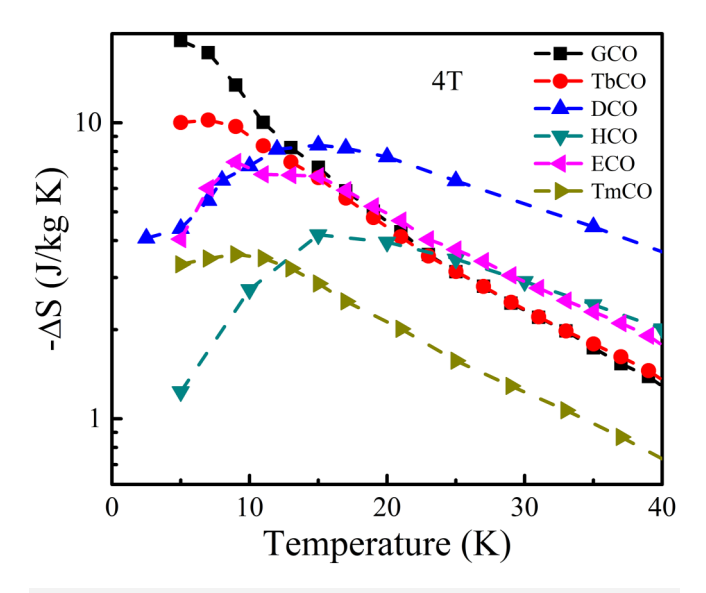


FIG. 7. Temperature dependence of the magnetic entropy change $(-\Delta S)$ under a magnetic field change of 4 T for the six RCrO₃ samples.

that $(-\Delta S)$ decreases rapidly with increasing temperature above 15 K for all the samples. The largest value of $(-\Delta S)$ in units of J kg⁻¹ K⁻¹ with a ΔH of 4 T is 19.0, 10.2, 8.4, 4.2, 7.4, and 3.6 for GCO, TbCO, DCO, HCO, ECO, and TmCO, respectively, and they occur at 5, 7, 15, 15, 9, and 9 K, respectively. The peak values of $(-\Delta S)$ of RCrO₃ below 20 K can be attributed to the complex magnetic interactions, such as Cr^{3+} – Cr^{3+} (spin reorientation), Cr^{3+} – R^{3+} (spin reorientation), and R^{3+} – R^{3+} (rare-earth ordering) at those temperatures.¹² It should be noted that for GCO, the continued increase in the $(-\Delta S)$ value with decreasing temperature to the lowest measured temperature of 5 K [with a maximum in $(-\Delta S)$ expected at around T_N^{Gd}] indicates the dominant contribution from the Gd³⁺-Gd³⁺ interaction.¹²

We next investigate any relationship between the magnitudes of $(-\Delta S)$ in RCrO₃ and the de Gennes factor (G) of rare earths R. The de Gennes factor, G, is defined using the following equa-

$$G = (g-1)^2 J(J+1),$$
 (5)

where g is the Landé g factor and J is the total angular momentum quantum number of trivalent R-ion.³⁹ The conventional G indicates the exchange interaction given by the inner product of the effective spin components of ions of the same kind. 40 It was found that the MCE of single crystal alloys of rare-earth metals at their respective magnetic ordering temperatures in a field directed along the easy magnetization axis depends linearly on the concentration of the magnetic ions and $G^{2/3}$, where G is defined by Eq. (5). 39,4 The magnetic ordering temperatures are expected to scale with the de Gennes factor G for isostructural rare-earth intermetallic compounds within the RKKY (Ruderman–Kittel–Kasuya–Yosida) model.⁴² This dependence was first proposed in work by $\frac{2}{6}$ Weinstein *et al.*,⁴³ but tested in the case of rare-earth alloys^{44,45} and $\frac{2}{6}$ recently in rare-earth metals.⁴⁶ In the present study, the validity of this relation and the dependence of change in entropy at T_N on the $G^{2/3}$ was experimentally tested for the present RCrO₃ materials. The rare-earth ordering temperature, T_N^R , for RCrO₃ has been collected from the literature and listed together with its corresponding G and $(-\Delta S)$ in Table II. The dependence of $(-\Delta S)$ at T_N^R on $G^{2/3}$ is plotted in Fig. 8. It should be noted that the value of $(-\Delta S)$ for GCO in Table II was taken at 5 K instead of 2.3 K due to limitation of measurable temperature range of PPMS and lack of data from the literature. It can be observed from Fig. 8 that $(-\Delta S)$ at T_N^R shows a generally linear dependence on $G^{2/3}$. This could possibly imply that the variation of the energy of the exchange interaction under a field provides a significant contribution to the variation of

TABLE II. Rare-earth ordering temperature T_N^R , de Gennes factor G, and magnetic entropy change $(-\Delta S)$ at T_N^R are listed here.

	GCO	TbCO	DCO	HCO	ECO	TmCO
T_N^R (K)	2.347	5.0 ¹⁶	3.8 ¹⁶	7.5 ⁴⁸	6.549	5 ⁵⁰
G	15.75	10.50	7.08	4.50	2.55	1.17
$(-\Delta S)$	18.96 ⁴	10.03	4.28^{24}	1.85^{20}	5.34^{17}	3.32



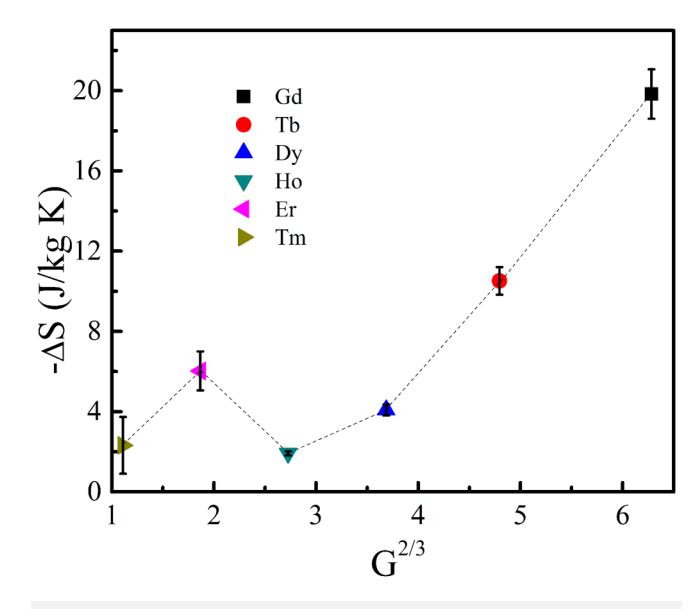


FIG. 8. The dependence of the magnetic entropy change $(-\Delta S)$ in RCrO₃ at the rare-earth ordering temperature on the de Gennes factor raised to the two thirds power, $G^{2/3}$. The dotted line connecting the data points is a visual guide.

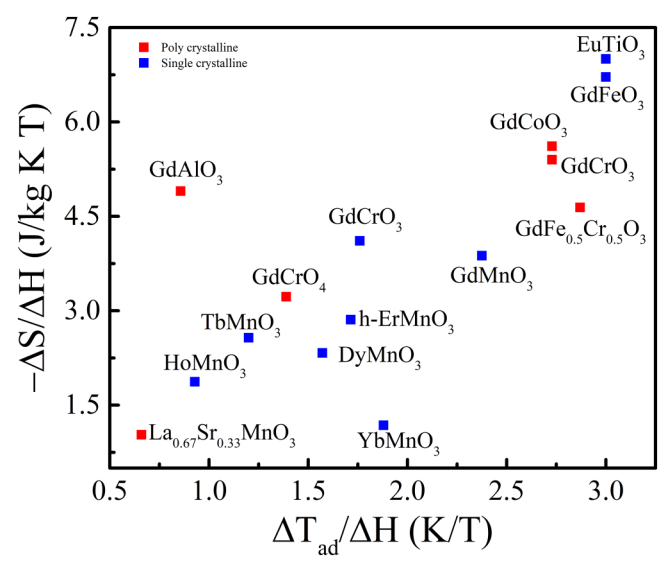


FIG. 9. Comparison of relative adiabatic temperature ($\Delta T_{\rm ad}/\Delta H$) and relative isothermal magnetic entropy change ($-\Delta S/\Delta H$) of some rare-earth oxide compounds.

entropy, and the exchange interaction can be attributed mainly to the R³⁺-R³⁺ exchange interaction.³⁹

D. Comparison of MCE for different systems

Among the studied six samples of RCrO $_3$ reported here, GdCrO $_3$ (GCO) shows the largest ($-\Delta S$) at 5 K (Figs. 7 and 8) making it a promising candidate for magnetic refrigeration. To better assess its potential in magnetic refrigeration among other rare-earth oxides, a survey on the comparison of MCE in rare-earth

oxides is given in Table III and plotted in Fig. 9. In several recent studies of the MCE in single crystals, ^{53,57,61,63} it has been depicted that MCE is highly anisotropic, the largest effect often observed for H parallel to the easy axis. In Table III, we have included reported numbers for polycrystals as well as for single crystals, the number listed for the latter are maximum values. In a recent paper, Balli et al. have exploited this anisotropy of MCE in single crystals of hexagonal ErMnO₃ by rotating the crystal between easy and hard directions in a constant magnetic field leading to unusual and large rotational MCE. ⁶¹

TABLE III. MCE properties of some rare-earth oxides from the literature.

Material	Crystalline	$-\Delta S$ (J/kg K)	ΔT_{ad} (K)	Reference
GdFeO ₃	Single	47.0 (7 T, 2.5 K)	21.0 (7 T, 5 K)	51
$GdFe_{0.5}Cr_{0.5}O_3$	Poly	32.5 (7 T, 6 K)	20.1 (7 T, 6 K)	21
GdCrO ₃	Poly	37.8 (7 T)	19.1 (7 T)	52
GdCrO ₃	Single	57.5 (14 T, 6 K)	24.7 (14 T, 16 K)	53
GdCrO ₄	Poly	29.0 (9 T, 22 K)	12.5 (9 T, 22 K)	54
GdAlO ₃	Poly	34.3 (7 T)	6.0 (7 T)	55
GdCoO ₃	Poly	39.3 (7 T)	19.1 (7 T)	55
$GdMnO_3$	Single	31.0 (8 T, 7 K)	19.0 (8 T, 19 K)	56
TbMnO ₃	Single	18.0 (7 T)	6.0 (5 T)	57 and 58
HoMnO ₃	Single	13.1 (7 T)	6.5 (7 T)	57 and 59
DyMnO ₃	Single	16.3 (7 T)	11.0 (7 T)	57 and 60
h-ErMnO ₃	Single	20.0 (7 T, 10 K)	12.0 (7 T)	61
$La_{0.67}Sr_{0.33}MnO_3$	Poly	5.2 (5 T, 370 k)	3.3 (5 T)	62
YbMnO ₃	Single	9.42 (8 T, 8 K)	15 (8 T, 8 K)	57
EuTiO ₃	Single	49 (7 T, 6 K)	21 (7 T, 6 K)	63

In Table III, two quantitative characteristics of MCE, adiabatic temperature change (ΔT_{ad}) and magnetic entropy change ($-\Delta S$), have been listed together with their corresponding magnetic field change and temperature. In Fig. 9, relative adiabatic temperature change ($\Delta T_{\rm ad}/\Delta H$) vs relative magnetic entropy change ($-\Delta S/\Delta H$) are plotted. The best candidates are single crystal of EuTiO3 and GdFeO₃ exhibiting a ΔT_{ad} of 21.0 K and a (- ΔS) of 49.0 J/kg K, and a $\Delta T_{\rm ad}$ of 21.0 K and a $(-\Delta S)$ of 47.0 J/kg K, respectively, under a field variation of 7 T.^{51,63} It is important to note that both Eu²⁺ and Gd3+ have the same spin configuration, resulting in a shared de Gennes factor. Additionally, Gd-containing oxides generally show superior MCE properties compared to other rare-earth oxides (Fig. 9). It could be inferred from this study that perovskite oxides containing rare-earth elements with a spin configuration similar to Gd may display competitive MCE performance in magnetic refrigeration. The MCE of rare-earth oxides at cryogenic temperatures may be attributed to the rare-earth itself (probably the G factor since Gd and Eu exhibit largest value of G among the other rare earths). This information could guide the designing of desirable materials with high MCE in cryogenic temperature ranges.

IV. CONCLUDING REMARKS

In this study, we have summarized the magnetic and magnetocaloric properties of series of high-quality samples of polycrystalline RCrO₃ (R = Gd, Tb, Dy, Ho, Er, and Tm) synthesized by a combustion reaction method. Magnetization measurements revealed that T_N^{Cr} of RCrO₃ decreases with decreasing ionic radii of R³⁺ ion. The modified Curie-Weiss law including Dzyloshinskii-Moriya (DM) interaction was used to fit the temperature dependence of susceptibility data above T_N^{Cr} . The symmetric exchange constant (J_e) was found to decrease, while the spin canting angle (α) was found to generally increase with the decreasing size of R³⁺ ion. Strong correlation is obtained between the magnetic entropy change $(-\Delta S)$ at T_N^R and $G^{2/3}$, where G is the de Gennes factor. Among RCrO₃, GdCrO₃ shows the largest value of $(-\Delta S/\Delta H)$, likely because of its largest G factor. This may indicate that the R3+-R3+ exchange interaction provides significant contribution to the magnetic entropy change $(-\Delta S)$ at T_N^R . The magnetocaloric properties of RCrO₃ are compared with those of other perovskitetype oxides and it is found that the magnitudes of $(\Delta T_{ad}/\Delta H)$ and $(-\Delta S/\Delta H)$ for GdCrO₃ compare well with the reported values for the perovskites GdFeO₃ and EuTiO₃. These comparisons presented here provide useful information on assessing the potential use of these materials in magneto-refrigeration technology.

ACKNOWLEDGMENTS

M.J. acknowledges the support of National Science Foundation EAGER Grants (Nos. CBET 2233149 and ECCS 2236879) as well as funding from UConn's Research Excellence Program for the work presented here.

AUTHOR DECLARATIONS

Conflict of Interest

The authors have no conflict to disclose.

Author Contributions

Jianhang Shi: Conceptualization (equal); Data curation (equal); Formal analysis (equal); Investigation (equal); Writing – original draft (equal); Writing – review & editing (equal). Mohindar S. Seehra: Formal analysis (equal); Methodology (equal); Writing – review & editing (equal). Jacob Pfund: Methodology (equal); Writing – review & editing (equal). Shiqi Yin: Data curation (equal). Menka Jain: Conceptualization (equal); Funding acquisition (equal); Project administration (equal); Resources (equal); Software (equal); Supervision (equal); Writing – review & editing (equal).

DATA AVAILABILITY

The data that support the findings of this study are available within the article.

REFERENCES

- ¹S. Wang, X. Wu, T. Wang, J. Zhang, C. Zhang, L. Yuan, X. Cui, and D. Lu, Inorg, Chem. **58**, 2315 (2019).
- ²J. Prado-Gonjal, R. Schmidt, J.-J. Romero, D. Ávila, U. Amador, and E. Morán, Inorg. Chem. **52**, 313 (2013).
- ³R. Mguedla, A. B. J. Kharrat, M. Saadi, K. Khirouni, N. Chniba-Boudjada, and W. Boujelben, J. Alloys Compd. 812, 152130 (2020).
- ⁴J. Shi, T. Sauyet, Y. Dang, S. L. Suib, M. S. Seehra, and M. Jain, J. Phys. Condens. Matter 33, 205801 (2021).
- ⁵J. Shi, G. W. Fernando, Y. Dang, S. L. Suib, and M. Jain, Phys. Rev. B **106**, 165117 (2022).
- ⁶V. S. Bhadram, D. Swain, R. Dhanya, M. Polentarutti, A. Sundaresan, and C. Narayana, Mater. Res. Express 1, 026111 (2014).
- ⁷G. N. P. Oliveira, A. L. Pires, P. Machado, A. M. Pereira, J. P. Araújo, and A. M. L. Lopes, J. Alloys Compd. 797, 269 (2019).
- ⁸R. Saha, A. Sundaresan, and C. N. R. Rao, Mater. Horiz. 1, 20 (2014).
- A. Ghosh, A. Pal, K. Dey, S. Majumdar, and S. Giri, J. Mater. Chem. C 3, 4162
- ¹⁰J. Shi, M. E. Johnson, M. Zhang, P.-X. Gao, and M. Jain, APL Mater. 8, 031106 (2020).
- ¹¹A. McDannald, S. Vijayan, J. Shi, A. Chen, Q. X. Jia, M. Aindow, and M. Jain, J. Mater. Sci. 54, 8984 (2019).
- ¹²L. H. Yin, J. Yang, X. C. Kan, W. H. Song, J. M. Dai, and Y. P. Sun, J. Appl. Phys. 117, 133901 (2015).
- ¹³M. L. Medarde, J. Phys. Condens. Matter **9**, 1679 (1997).
- ¹⁴B. S. Nagaraja, A. Rao, P. Poornesh, and G. S. Okram, J. Supercond. Novel Magn. 31, 2271 (2018).
- 15S. Catalano, M. Gibert, J. Fowlie, J. Iniguez, J.-M. Triscone, and J. Kreisel, Rep. Prog. Phys. 81, 046501 (2018).
- ¹⁶L. Yin, J. Yang, P. Tong, X. Luo, C. Park, K. Shin, W. Song, J. Dai, K. Kim, and X. Zhu, J. Mater. Chem. C 4, 11198 (2016).
- 17 J. Shi, S. Yin, M. S. Seehra, and M. Jain, J. Appl. Phys. 123, 193901 (2018).
- ¹⁸V. K. Pecharsky and K. A. Gschneidner, Jr., Phys. Rev. Lett. **78**, 4494 (1997).
- ¹⁹S. Yin, W. Zhong, C. J. Guild, J. Shi, S. L. Suib, L. F. Cótica, and M. Jain, J. Appl. Phys. **123**, 053904 (2018).
- S. Yin, T. Sauyet, M. S. Seehra, and M. Jain, J. Appl. Phys. 121, 063902 (2017).
 J. Shi, M. S. Seehra, Y. Dang, S. L. Suib, and M. Jain, J. Appl. Phys. 129, 243904 (2021)
- 22S. Yin, T. Sauyet, C. Guild, S. L. Suib, and M. Jain, J. Magn. Magn. Mater. 428, 313 (2017).
- ²³M. Fiebig, T. Lottermoser, T. Lonkai, A. V. Goltsev, and R. V. Pisarev, J. Magn. Magn. Mater. **290–291**, 883 (2005).
- ²⁴A. McDannald, L. Kuna, and M. Jain, J. Appl. Phys. **114**, 113904 (2013).

- 25 K. Yoshii, Mater. Res. Bull. 47, 3243 (2012).
- 26K. Yoshii, J. Appl. Phys. 126, 123904 (2019).
- ²⁷L. Holmes, M. Eibschütz, and L. G. Van Uitert, J. Appl. Phys. **41**, 1184 (1970).
- ²⁸S. Mahana, U. Manju, and D. Topwal, Complex Magnetic Behavior in GdCrO₃ (AIP Publishing LLC, 2017), p. 130046.
- ²⁹S. Mugiraneza and A. M. Hallas, Commun. Phys. 5, 95 (2022).
- 30W. K. Zhu, C.-K. Lu, W. Tong, J. M. Wang, H. D. Zhou, and S. X. Zhang, Phys. Rev. B 91, 144408 (2015).
- ³¹T. Moriya, Phys. Rev. **120**, 91 (1960).
- 32D. Treves, Phys. Rev. 125, 1843 (1962).
- 33X.-Y. Wang, Z.-M. Wang, and S. Gao, Inorg. Chem. 47, 5720 (2008).
- ³⁴N. Shamir, H. Shaked, and S. Shtrikman, Phys. B+C **90**, 211 (1977).
- 35 T. Kimura, S. Ishihara, H. Shintani, T. Arima, K. Takahashi, K. Ishizaka, and Y. Tokura, Phys. Rev. B 68, 060403 (2003).
- ³⁶E. Bousquet and A. Cano, J. Phys.: Condens. Matter 28, 123001 (2016).
- ³⁷A. McDannald, L. Kuna, M. S. Seehra, and M. Jain, Phys. Rev. B **91**, 224415
- 38Y. Su, J. Zhang, B. Li, B. Kang, Q. Yu, C. Jing, and S. Cao, Ceram. Int. 38, S421 (2012).
- 39 A. M. Tishin, J. Alloys Compd. 250, 635 (1997).
- 40Y. Hirayama, T. Nakagawa, and T. A. Yamamoto, Solid State Commun. 151, 1602 (2011).
- ⁴¹A. S. Andreenko, K. P. Belov, S. A. Nikitin, and A. M. Tishin, Sov. Phys. Usp. 32, 649 (1989).
- 42 L. Xue, L. Shao, Q. Luo, and B. Shen, J. Alloys Compd. 790, 633 (2019).
- ⁴³S. Weinstein, R. S. Craig, and W. E. Wallace, J. Appl. Phys. 34, 1354 (1963).
- 44R. M. Bozorth, J. Appl. Phys. 38, 1366 (1967).
- 45H. R. Child and J. W. Cable, J. Appl. Phys. 40, 1003 (1969).
- 46R. R. Gimaev, A. S. Komlev, A. S. Davydov, B. B. Kovalev, and V. I. Zverev, Crystals 11, 82 (2021).
- ⁴⁷A. H. Cooke, D. M. Martin, and M. R. Wells, J. Phys. C: Solid State Phys. 7, 3133 (1974).

- ⁴⁸S. Yuling, J. Zhang, F. Zhenjie, L. Zijiong, S. Yan, and C. Shixun, J. Rare Earths 29, 1060 (2011).
- 49 Y. Su, J. Zhang, L. Li, B. Li, Y. Zhou, D. Deng, Z. Chen, and S. Cao, Appl. Phys. A 100, 73 (2010).
- 50 T. Tamaki, K. Tsushima, and Y. Yamaguchi, Phys. B+C 86-88, 923 (1977).
- ⁵¹ M. Das, S. Roy, and P. Mandal, Phys. Rev. B **96**, 174405 (2017).
- 52S. Mahana, U. Manju, and D. Topwal, J. Phys. D: Appl. Phys. 51, 305002
- 53 Y. Zhu, P. Zhou, T. Li, J. Xia, S. Wu, Y. Fu, K. Sun, Q. Zhao, Z. Li, and Z. Tang, Phys. Rev. B 102, 144425 (2020).
- ⁵⁴E. Palacios, C. Tomasi, R. Sáez-Puche, A. J. Dos santos-García, F. Fernández-Martínez, and R. Burriel, Phys. Rev. B 93, 064420
- 55Q. Y. Dong, K. Y. Hou, X. Q. Zhang, L. Su, L. C. Wang, Y. J. Ke, H. T. Yan, and Z. H. Cheng, J. Appl. Phys. 127, 033904 (2020).
- 56 A. A. Wagh, K. Suresh, P. A. Kumar, and S. Elizabeth, J. Phys. D: Appl. Phys. 48, 135001 (2015).
- 57 A. Midya, S. N. Das, P. Mandal, S. Pandya, and V. Ganesan, Phys. Rev. B 84, 235127 (2011).
- 58J.-L. Jin, X.-Q. Zhang, G.-K. Li, Z.-H. Cheng, L. Zheng, and Y. Lu, Phys. Rev. B 83, 184431 (2011).
- 59 A. Midya, P. Mandal, S. Das, S. Banerjee, L. S. Chandra, V. Ganesan, and S. R. Barman, Appl. Phys. Lett. 96, 142514 (2010).
- 60 M. Balli, S. Mansouri, S. Jandl, P. Fournier, and D. Z. Dimitrov, Solid State Commun. 239, 9 (2016).
- 61 M. Balli, S. Jandl, P. Fournier, J. Vermette, and D. Z. Dimitrov, Phys. Rev. B 98, 184414 (2018).
- 62 A. Rostamnejadi, M. Venkatesan, P. Kameli, H. Salamati, and J. M. D. Coey, J. Magn. Magn. Mater. 323, 2214 (2011).
- J. Magn. Magn. Mater. 323, 2214 (2011).

 63 A. Midya, P. Mandal, K. Rubi, R. Chen, J.-S. Wang, R. Mahendiran, G. Lorusso, and M. Evangelisti, Phys. Rev. B 93, 094422 (2016).